buildings

MDPI

Article

Joint Action of Wind and Temperature on Long-Span Concrete-Filled Steel Tube Bridges in the Yellow River Basin

Jiang Liu [1], Haotian Wu [1], Huajun Guo [2], Zhiyuan Ma [1], Feixiang Zheng [1], Yinping Ma [3,*] and Yongjian Liu [1,3,*]

[1] School of Highway, Chang'an University, Xi'an 710064, China
[2] Qinghai Provincial Transportation Construction Management Co., Ltd., Xi'ning 810000, China
[3] School of Civil Engineering, Chongqing University, Chongqing 400044, China
* Correspondence: myfmy1@cqu.edu.cn (Y.M.); liuyongjian@chd.edu.cn (Y.L.)

Abstract: Complex wind and temperature characteristics in the Yellow River basin (YRB) challenge the safety and durability of long-span concrete-filled steel tube (CFST) bridges greatly. To address this issue, it is important to accurately assess the joint actions of wind and temperature. In this paper, the joint actions of wind and temperature in eight typical YRB cities are analyzed. The joint distributions of wind speed and air temperature are developed with the Archimedean Copula, and the Kendall return period is used for occurrence probability estimations. Eight wind–temperature combinations are considered. Responses for these combinations are calculated and compared with specification actions. Results show significant wind–temperature variations in the YRB. When wind actions adopt the univariate representative values (URVs), the temperature actions are reduced by 20–40%; when temperature actions use URVs, wind actions experience a reduction by more than half of their URVs. The joint responses can sometimes exceed, but are mostly less than, the specification responses, with a maximum strength margin over 11 MPa. These efforts suggest that the proposed joint actions can expand the provisions in the General Specification and provide guidance for the design of long-span CFST bridges.

Keywords: CFST bridges; wind action; temperature action; the Yellow River basin; joint action; joint effect; copula

check for updates

Academic Editor: Antonio Formisano

Received: 23 December 2024
Revised: 10 February 2025
Accepted: 17 February 2025
Published: 18 February 2025

Citation: Liu, J.; Wu, H.; Guo, H.; Ma, Z.; Zheng, F.; Ma, Y.; Liu, Y. Joint Action of Wind and Temperature on Long-Span Concrete-Filled Steel Tube Bridges in the Yellow River Basin. *Buildings* **2025**, *15*, 633. https://doi.org/10.3390/buildings15040633

Copyright: © 2025 by the authors. Licensee MDPI, Basel, Switzerland. This article is an open access article distributed under the terms and conditions of the Creative Commons Attribution (CC BY) license (https://creativecommons.org/licenses/by/4.0/).

1. Introduction

The Yellow River, the second longest river in China, is known as the mother river of China. It spans a diverse range of geomorphological zones, encompassing the Qinghai–Tibet Plateau, the Inner Mongolia Plateau, the Loess Plateau, and the Huang-Huai-Hai Plain. This extensive geographical diversity contributes to the complex wind and temperature characteristics of the Yellow River basin (YRB). The geolocation of the YRB is displayed in Figure 1. These complex wind–temperature characteristics have profound impacts on joint wind–temperature values, leading to great diversity in the joint action of wind and temperature in the YRB. In the meantime, with the rapid economic and social development of the YRB, there is an urgent need for the advancement of transport infrastructure, and bridge construction is in full swing. Among bridges, concrete-filled steel tube (CFST) bridges exhibit remarkable advantages, including superior spanning capabilities, favorable mechanical properties, strong resistance ability in harsh environments, and excellent economic benefits. These advantages give a great impetus to increasing the construction of long-span CFST bridges in the YRB. This trend underscores the growing demand for safe and economical solutions in the region's CFST bridges design. Wind and temperature actions are important factors to be considered in design, as they significantly impact the

safety and durability of CFST bridges [1–3]. Ignorance of the dependence between wind and temperature actions would result in a misunderstanding of risk. Therefore, accurate estimations of their joint actions are essential for addressing the challenges posed by the complicated environmental conditions in the YRB.

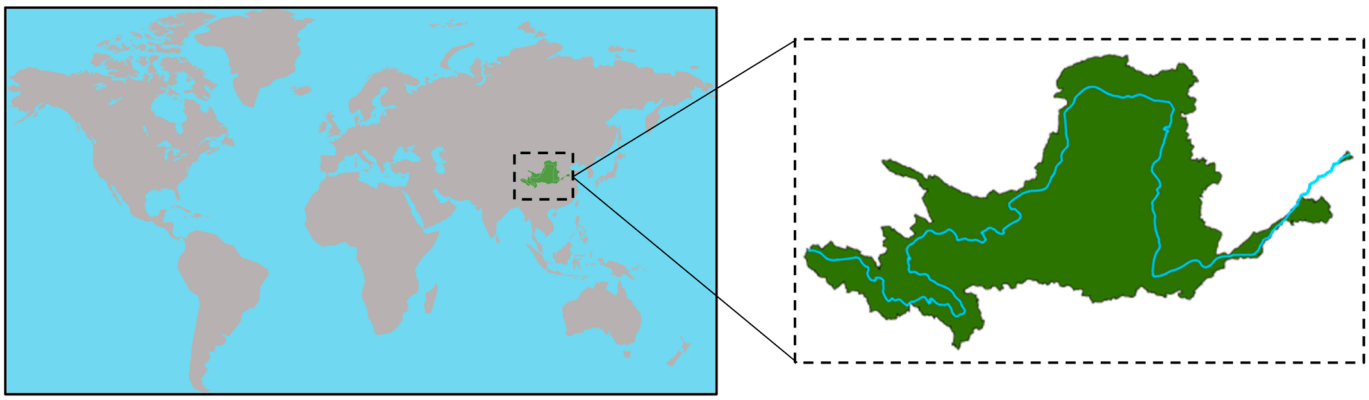


Figure 1. Geolocation of YRB.

In the current specifications [4–7], joint wind–temperature actions are considered through action combinations. A superposition of the maximum values of wind and temperature actions is used in the Code for Design on Railway Bridge and Culvert (Railway Code) [5]; this overestimates their joint actions, causing material waste. The General Specifications for Design of Highway Bridges and Culverts (General Specification) [4] state that when wind action is taken as the main variable action, the combination coefficient for temperature action is 0.75. In addition, as is stipulated in the Wind-resistant Design Specification for Highway Bridges (Wind-resistant Specification) [6], wind action takes the representative value with a return period of 100 a in this case. Meanwhile, when temperature action is specified as the main variable action, the wind action coefficient is 1. And a wind action value with a return period of 10 a is adopted here. Similarly, the Eurocode [7] stipulates that for the serviceability limit state of railway bridges, temperature action is reduced to 0.6 when the wind is the main variable action, while wind action is reduced to 0.75 when temperature is the main variable action. The aforementioned four coefficients are derived from long-term empirical cumulative correction [8]. The correlation between wind and temperature actions is not considered. Additionally, the wind and temperature characteristics of the YRB exhibit great diversity. Unified coefficient values are not appropriate for the joint wind–temperature action in the YRB. Providing more detailed coefficient values is urgently needed.

Wind speed is typically used to represent wind action [6]. In this paper, uniform temperature action (the temperature change of the bridge) is adopted for temperature action. It encompasses uniform heating action (UHA) (elevation in bridge temperature) and uniform cooling action (UCA) (drop in bridge temperature), which can be obtained from the correlation with air temperature [9]. Hence, exploration of the joint distribution of wind speed and air temperature is crucial for accurately estimating the joint wind–temperature action in YRB.

Copula theory provides an excellent tool for the construction of the joint distribution of wind speed and air temperature by connecting both marginal distributions together [10]. It exhibits a great deal of advantages in statistical modeling. When developing the joint distribution of random variables, copulas do not impose any specific requirements on their marginal distributions, thereby providing great flexibility in modeling [11,12]. In addition, this approach can also reduce the uncertainties of the statistical properties to be estimated [13].

Copulas, originated from Sklar's theorem [14], have been applied in numerous domains, including water resources [15–17], civil engineering, and so on. In civil engineering, copulas are mainly used to assess the multivariate risk of structural safety [18–20]. With regard to the fields related to this paper, in wind engineering, studies mainly concentrate on the correlation among wind environment parameters, such as the joint distribution of wind speed and wind direction [21,22] and the joint distribution of wind speed, wind direction, and wind attack angle [23,24]. In relation to temperature action, copulas are introduced to investigate the temperature distribution of the girder [25,26]. When it comes to the topic of this paper, Wang et al. [27] and Zhang et al. [28] proposed an approach to assess the joint wind–temperature action on long-span bridges. Ding et al. [29] constructed the joint distribution of wind speed and air temperature using SHM data on Jiashao bridge. Zhou et al. [30] investigated the correlation between wind speed and temperature of a composite girder bridge during typhoon Lekima. The aforementioned studies mainly concentrate on specific coastal cable-stayed bridges, and none of them focus on the joint wind–temperature action on long-span CFST bridges in the YRB. CFST bridges have distinct structural characteristics compared to other types of bridges, such as different material properties and structural responses to wind–temperature actions. The YRB also has its own unique climatic and geographical conditions. The wind–temperature environment in this region can be significantly different from coastal areas, which may lead to specific patterns of joint wind–temperature action. In addition, the regional differences in joint wind–temperature action have also not been studied. Therefore, it is necessary to investigate joint wind–temperature action on long-span CFST bridges in the YRB.

In this paper, considering the correlation between wind and temperature actions, joint wind–temperature actions are studied for long-span CFST bridges in the YRB. First, eight cities are selected to represent the typical environmental conditions in the YRB. Then, the Archimedean Copula is introduced to develop the joint distributions of wind speed and air temperature, and the Kendall return period (KRP) is adopted to assess the possibility of occurrence for wind and temperature actions. Next, assuming the bivariate return period equals the univariate one, eight potential combinations of the joint action are determined. After that, the responses of the joint actions are calculated for the eight combinations separately. And a comparative analysis is made between different cities, as well as specification actions.

2. Methods

2.1. General Flowchart

A general flowchart illustrating the methodology utilized in this paper is presented in Figure 2. In order to investigate the joint wind–temperature action on long-span CFST bridges in the YRB, the initial step is deriving the joint distribution of wind speed and air temperature at the site. Subsequently, the joint values of these actions are estimated using KRP. The detailed process includes the following five procedures: Firstly, cities representing typical wind and temperature conditions in the YRB are selected. Secondly, long-term meteorological data in these cities are collected. And then they are processed into monthly extreme value samples. Subsequently, these samples are divided into two parts, i.e., the hot one and the cold one. Thirdly, generalized extreme value distribution (GEV) is utilized to derive the marginal distributions of wind speed and air temperature. Fourthly, the dependence structures between wind speed and air temperature are developed using the Archimedean Copula. Assuming a bivariate return period equals the univariate one, the contours of the joint distributions can be obtained. Then, the wind speeds and air temperatures are transformed into wind actions and temperature actions. Finally, the joint values and combination coefficients of wind and temperature actions are acquired.

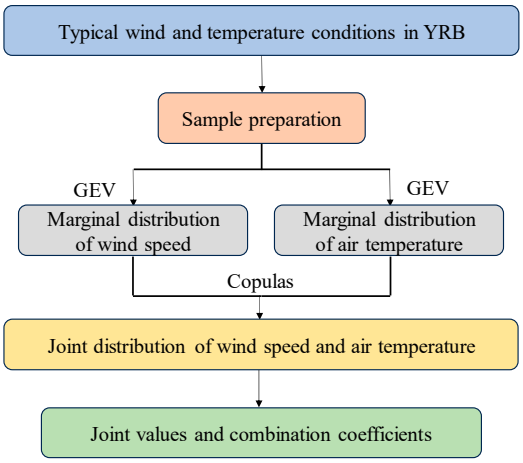


Figure 2. Flowchart. Note: GEV denotes generalized extreme value distribution.

2.2. Typical Wind and Temperature Conditions in the Yellow River Basin

The Yellow River, the second longest river in China, holds a multifaceted significance for China; it is known as the mother river of China [31]. The river originates in the Bayan Har Mountains in the Qinghai–Tibet Plateau and flows eastward until it empties into the Bohai Sea, passing through various terrains such as plateaus, mountains, hills, and plains. The total length of the Yellow River is about 5464 km, and the area of the YRB spans approximately 795,000 km^2, as seen in Figure 3a. The elevation difference in the YRB is quite large, with the western regions being considerably higher than the eastern ones. In addition, the YRB, located in the middle latitude zone, is greatly affected by complicated atmospheric circulation and monsoon circulation. This varied topography and complex thermal circulation contribute to the diverse wind and temperature characteristics of the YRB.

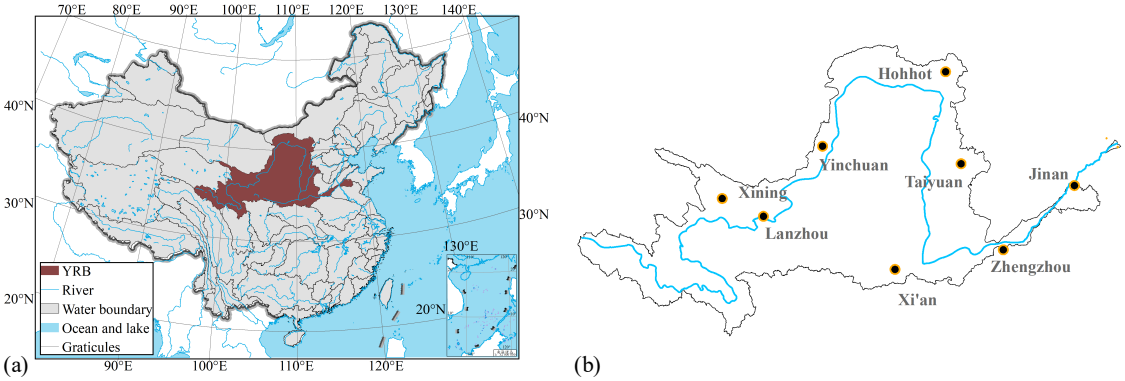


Figure 3. Geolocation of YRB and its typical cities: (**a**) geolocation of YRB; (**b**) geolocation of typical cities in YRB.

The YRB mainly exhibits the climatic characteristics of temperate continental climate and temperate monsoon climate and experiences significant seasonal temperature fluctuations. Winter is typically cold, while summer can be quite hot. Wind speeds are mostly influenced by the topographical variations. In the mountainous area, wind speed is significantly accelerated due to narrow tube effect [32], with prevailing winds often originating from the west and northwest. The average wind speeds can be over 6.0 m/s, while the extreme values even exceed 26.8 m/s [33]. In areas with relatively flat terrain, wind speed is generally more subdued, with average wind speeds of about 3.0 m/s and extreme wind

speeds of 17.0 m/s or so [33]. Moreover, the YRB receives substantial solar radiation, particularly during the summer months.

In summary, considering the wind speed and air temperature characteristics as well as the geographic information (longitude, latitude, elevation, and topography), eight cities were selected to represent the typical characteristics of the YRB, as seen in Figure 3b. More details are given in Table 1. The selected sites are evenly scattered along the Yellow River, covering the main economic zones of the YRB. Among these cities, Xining holds a plateau alpine cold temperature climate, with high wind speed and low air temperature. Lanzhou, Yinchuan, and Hohhot belong to the temperate continental climate zone, which is characterized by long and cold winters and short but hot summers. Zhengzhou and Jinan have obvious features of a temperate monsoon climate. Under the influence of varying atmospheric circulation patterns, the region experiences distinct seasonal climatic variations characterized by warm springs, hot summers, cool autumns, and cold winters.

Table 1. Information about the eight typical cities.

Cities	Provinces	Longitudes	Latitudes	Elevation	Topography	Wind–Temperature Characteristics
Xining	Qinghai	101.45°	36.44°	2295.2 m	Plateau	Strong winds and cold winters
Lanzhou	Gansu	104.41°	36.34°	1398.2 m	Valley	Strong winds, hot summers, and cold winters
Yinchuan	Ningxia	106.12°	38.28°	1110.9 m	Mountain and plain	Strong winds, hot summers, and cold winters
Hohhot	Inner Mongolia	111.34°	40.51°	1153.5 m	Plateau	Strong winds and cold winters
Taiyuan	Shanxi	112.35°	37.37°	776.3 m	Basin	Moderate winds, hot summers, and cold winters
Xi'an	Shaanxi	108.58°	34.26°	410.0 m	Plain and hills	Moderate winds, hot summers, and cold winters
Zhengzhou	Henan	113.39°	34.43°	110.4 m	Plain	Moderate winds, hot summers, and cold winters
Jinan	Shandong	117.00°	36.36°	170.3 m	Plain and hills	Light winds, hot summers, and cold winters

2.3. Marginal Distribution

Before establishing the joint distribution, marginal distributions should be obtained first. Wind speed and air temperature usually follow skewed distributions in extreme value analysis. GEV has flexible shape parameters, allowing it to capture such asymmetric behavior of extreme values. It can handle the fact that extreme values may not follow the same pattern as the bulk of the data and can account for the skewness that often arises when considering only the extreme values. Therefore, in this study, GEV is used to characterize the distributions. The cumulative distribution function (CDF) of GEV can be expressed as [34]

$$F(x;\mu,\sigma,k) = \exp\left\{-\left(1+k\frac{x-\mu}{\sigma}\right)^{-1/k}\right\},\ 1+k(x-\mu)/\sigma > 0 \quad (1)$$

where k is the shape parameter; μ is the location parameter; σ is the scale parameter.

2.4. Joint Distribution

The joint distribution of wind speed and air temperature is constructed via copulas. Copula theory originates from Sklar's theorem [14] and is implemented by Joe [35] and Nelson [36]. It notes that an n-dimensional joint distribution function can be expressed by a copula function and marginal distribution functions, where the copula function represents the correlation between the variables. For two-dimensional cases, the joint cumulative distribution function (JCDF) can be expressed as

$$H(x, y) = C(F(x), G(y)) \tag{2}$$

where X and Y are the random variables; C is the copula function; $F(x)$ and $G(y)$ are the cumulative density functions of X and Y, respectively. Accordingly, the joint probability density function (JPDF) is as follows:

$$h(x, y) = c(F(x), G(y)) f(x) g(y) \tag{3}$$

where c is the density function of C; $f(x)$ and $g(y)$ are the CDFs of X and Y.

2.4.1. Archimedean Copula

The Archimedean Copula has many advantages in the establishment of joint distributions. It is capable of describing a wide variety of dependence relationships among variables for diverse dependence structures. In addition, it excels in characterizing the tail dependence of variables. Tail dependence refers to the mutual dependence of variables in the tails of the distribution (the extreme value parts). Moreover, the Archimedean Copula has a concise parametric form, which facilitates the estimation and fitting of the model greatly. Thus, this study utilizes the Archimedean Copula for the construction of the joint distribution.

Let φ be a continuous and strictly monotonically decreasing convex function, $\varphi(1) = 0$, $\varphi^{[-1]}$: $[0, \infty] \rightarrow [0, 1]$ is the pseudo-inverse function of φ

$$\varphi^{[-1]}(t) = \begin{cases} \varphi^{-1}(t), & 0 \leq t \leq \varphi(0) \\ 0, & \varphi(0) \leq t \leq \infty \end{cases} \tag{4}$$

In this way, the copula function can be expressed as

$$C(u, v) = \varphi^{[-1]}(\varphi(u), \varphi(v)) \tag{5}$$

where C is the Archimedean Copula; $u = F(x)$, $v = G(y)$; φ is the generator of the Archimedean Copula. According to types of generators, three typical one-parameter Archimedean Copulas, namely, Gumbel–Hougaard (Gumbel) Copula, Cook–Johnson (Clayton) Copula, and Frank Copula, are listed in Table 2.

Table 2. Typical one-parameter Archimedean Copulas.

Copulas	$\varphi(t)$	$C(u, v)$	Range of Parameter θ
Gumbel	$(-\ln t)^{\theta}$	$\exp\left\{-[(-\ln u)^{\theta} + (-\ln v)^{\theta}]^{1/\theta}\right\}$	$[1, +\infty)$
Clayton	$\left(t^{-\theta} - 1\right)/\theta$	$\max\left\{\left(u^{-\theta} + v^{-\theta} - 1\right)^{-1/\theta}, 0\right\}$	$(0, +\infty)$
Frank	$-\ln[(e^{-\theta t} - 1)/(e^{-\theta} - 1)]$	$-\frac{1}{\theta}\ln[1 + \frac{(e^{-\theta u} - 1)(e^{-\theta v} - 1)}{(e^{-\theta} - 1)}]$	$(-\infty, 0) \cup (0, +\infty)$

2.4.2. Parameter Estimations

Parameter estimation is vital to the construction of copulas, directly affecting the accuracy of the expected model. Maximum likelihood estimation provides desirable properties in parameter estimations, such as consistency and efficiency. In addition, it can effectively capture the characteristics of the data. However, unlike Bayesian methods, the lack of prior information utilization can be a disadvantage for maximum likelihood estimation. In this paper, maximum likelihood estimation is introduced for parameter estimation of Archimedean Copulas due to its good convergence properties and ease of implementation.

Let X and Y be n-dimensional continuous random variables with marginal distribution functions $u = F(x)$ and $v = G(y)$, joint distribution function $C(u, v)$, and parameter θ. The likelihood function can be expressed as

$$L(\theta) = \prod_{i=1}^{n} c(u(i), v(i); \theta) \tag{6}$$

then, the expected parameter value can be solved from

$$\frac{\partial \ln(L(\theta))}{\partial \theta} = 0 \tag{7}$$

2.4.3. Goodness-of-Fit Tests

The empirical copula [37], based on observed data, is employed to select the best-fitted copula from the expected ones. It is defined as

$$C\left(\frac{i}{n}, \frac{j}{n}\right) = \frac{p}{n} \tag{8}$$

where p is number of pairs when $x_t \leq x_{(i)}$, $y_t \leq y_{(j)}$; (x_t, y_t) is a pair of sample value, $t = 1, \ldots, n$; n is the sample size; $x_{(i)}, y_{(j)}$ is the order statistics in each sample vector, $1 \leq i, j \leq n$.

The root mean square error (RMSE) and Bayesian Information Criterion (BIC) are utilized to test the goodness-of-fit of expected copulas. The best-fitted model should exhibit the lowest values of RMSE and BIC.

RMSE represents the sample standard deviation of the difference between the expected values and empirical values, revealing the difference between the expected model and empirical model. It is listed below:

$$\mathrm{RMSE} = \sqrt{\mathrm{MSE}} = \sqrt{\frac{1}{n}\sum_{i=1}^{n}\left(C_{\mathrm{exp}}(i) - C_{\mathrm{emp}}(i)\right)^2} \tag{9}$$

where C_{exp} and C_{emp} denote the expected copula and empirical copula, respectively.

BIC [38] is a criterion for model selection which balances the goodness-of-fit and complexity of the model to select the best model. It can be expressed as

$$\mathrm{BIC} = n\sqrt{\mathrm{MSE}} + k \ln n \tag{10}$$

where k represents the number of independently adjusted parameters within the model.

2.5. Joint Values and Combination Coefficients for Wind and Temperature Actions

2.5.1. Kendall Return Period (KRP)

In the joint analysis of two random variables X and Y, a binary dangerous event can be defined as the joint distribution value of X and Y that exceeds the specified probability level.

Accordingly, a bivariate return period can be expressed by the KRP [39]. The definition of the KRP is as follows

$$T^K = \frac{\mu_T}{\mathrm{P}\{C(F(x), G(y)) > t\}} = \frac{\mu_T}{1 - K_C(t)} \tag{11}$$

where μ_T represents the span of time interval between two consecutive extremes, and it takes 1/12 year in this paper; $K_C(t)$ is Kendall's measure of Copula C, which is given by

$$K_C(t) = \mathrm{P}\{C(u, v) \leq t, 0 < t \leq 1\} = t - \varphi(t)/\varphi'(t) \tag{12}$$

2.5.2. Joint Values and Combination Coefficients

With the concept of the KRP, the joint values of wind and temperature actions can be obtained, and they are expressed in the form of contours of joint distributions of wind speed and air temperature. Assuming that a bivariate return period equals a univariate return period, for a certain return period, when one variable is specified to its univariate representative value, the other variable can be determined, and the value will be smaller than its URV [27].

Prior to the determination of the joint values, it is essential to first obtain their univariate representative values. The Wind-resistant Specification [6] stipulates two levels of wind actions. The action with a return period of 10 a is called W1, and the other with a return period of 100 a is called W2. Notably, W2 is adopted only when the wind action is specified as the main variable action [6]. When the temperature action is specified as the main variable action, W1 is employed. As for temperature action, no specific provisions about its return period are given in the General Specification [4]. The Eurocode [7] adopts a 50-year return period for temperature action. Considering the design reference period of 100 a, a return period of 100 a is adopted for temperature action in this paper.

After the joint value determination, the concept of combination coefficient can be defined as the ratio of the reduced action to the specified action:

$$\omega = \frac{\text{Reduced action}}{\text{Specified action}} = \begin{cases} \frac{\text{Reduced } U_z}{\text{Specified } U_z} = \frac{\text{Reduced } (z/10)^{\alpha} U_{10}}{\text{Specified } (z/10)^{\alpha} U_{10}} = \frac{\text{Reduced } U_{10}}{\text{Specified } U_{10}} \\ \frac{\text{Reduced uniform temperature action}}{\text{Specified uniform temperature action}} = \frac{\text{Reduced } T_e - T_0}{\text{Specified } T_e - T_0} \end{cases} \tag{13}$$

where U_z is the wind speed at a height of z m above the ground; α is the terrain roughness coefficient, which takes 0.3 for the convenience of calculation and subsequent comparison; U_{10} is the wind speed at a height of 10 m above the ground; T_e is effective temperature; T_0 is closure temperature.

Several types of action combination are proposed in Table 3. Specified actions, reduced actions, and combination coefficients are displayed. Notably, there exist two levels of wind actions (W1 and W2). Return periods of 10 a and 100 a are utilized in this paper.

Table 3. Types of action combination.

Combinations	Specified Actions	Reduced Actions	Bivariate Return Periods
C1	Specified W1	Reduced UHA	10 a
C2		Reduced UCA	10 a
C3	Specified W2	Reduced UHA	100 a
C4		Reduced UCA	100 a
C5	Specified UHA	Reduced W1	10 a
C6		Reduced W2	100 a
C7	Specified UCA	Reduced W1	10 a
C8		Reduced W2	100 a

3. Case Study

3.1. Background

Jishixia Grand Bridge, the longest CFST arch bridge in northwest China, is selected as the case study. The total length of the bridge is 492 m, incorporating a 265 m deck CFST arch bridge with a rise–span ratio of 1/5.5 and several 30 m prestressed concrete box girders, as shown in Figure 4.



Figure 4. Rendering of Jishixia Grand bridge.

Assuming the bridge is constructed in the aforementioned cities, the joint wind–temperature action can be obtained. Limited by the length of the article, only the process conducted for Xining is displayed in detail. The results for other cities will be given in Section 4.

3.2. Sample Preparation

Before the analysis, the initial meteorological data from 1953 to 2015 at Xining Station were received first. Then, the datasets were preprocessed and the wrong values and outliers were removed. Box plots were introduced for the removal, and points lower than "Q1 (lower quartile) − 1.5 IQR (interquartile range)" or greater than "Q3 (upper quartile) + 1.5 IQR" were removed.

After the preprocessing, the monthly extreme values and their accompanying values were selected. Considering the temperature action incorporates heating and cooling actions, the joint wind–temperature action can be divided into the combination of wind and heating actions and that of wind and cooling actions. Therefore, based on the principle that one action is specified as the main action and the other is reduced, the wind and temperature samples can be categorized into three distinct types, namely, "maximum wind speed group (maximum wind speed and accompanying air temperature)", "maximum air temperature group (maximum air temperature and accompanying wind speed)", and "minimum air temperature group (minimum air temperature and accompanying wind speed)". Maximum UHA and UCA regularly take place in hot and cold months. This approach may incorporate too many useless samples. In addition, the joint distribution in this case usually presents multimodal features, which is unfavorable for subsequent analysis. Therefore, it is necessary to explore a more thorough grouping strategy.

Given the occurrence possibility of maximum UHA and UCA, the three types of samples were subdivided by hot and cold months. To ensure an adequate sample size, both parts incorporate six months in one year. After several attempts, the months from April to September were designated as the hot months, while the other months were specified as the cold months. The samples after grouping are shown in Figure 5. The red scatters and curves denote the samples in the hot months, while the blue ones represent the samples in the cold months. It can be known that there exist distinctive boundaries between the scatters in

the hot and cold months for the three types of samples. In addition, the kernel smoothing curves also show a unimodal distribution characteristic, which facilitates the modeling of the marginal distributions. Therefore, the adopted grouping strategy can prove favorable for both the analysis of UHA and UCA and the construction of marginal distributions.

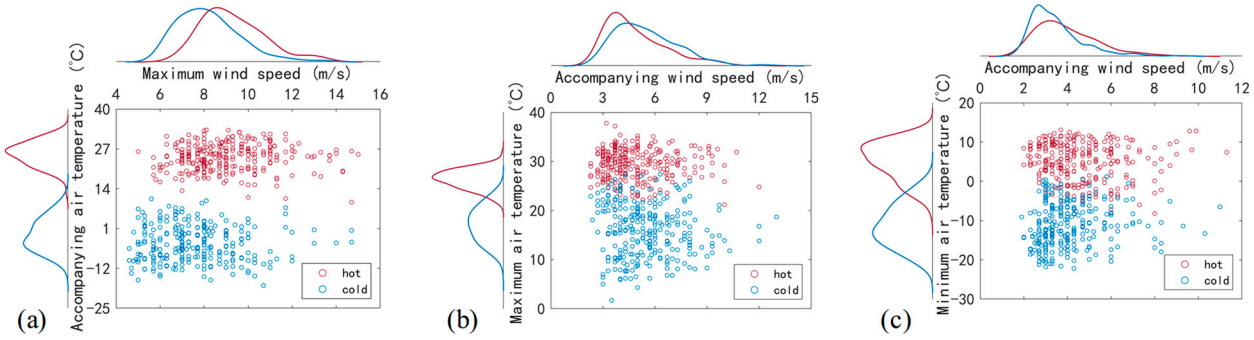


Figure 5. Grouped marginal diagrams for wind speed and air temperature: (**a**) maximum wind speed group; (**b**) maximum air temperature group; (**c**) minimum air temperature group.

However, the maximum air temperature in the cold months and minimum air temperature in the hot months do not make sense, because they cannot represent the maximum UHA and UCA. Hence, four groups are retained in the end:

1. $G_{WS\text{-}H}$: maximum wind speed and accompanying air temperature in the hot months.
2. $G_{WS\text{-}C}$: maximum wind speed and accompanying air temperature in the cold months.
3. $G_{AT\text{-}H}$: maximum air temperature and accompanying wind speed in the hot months.
4. $G_{AT\text{-}C}$: minimum air temperature and accompanying wind speed in the cold months.

3.3. Marginal Distribution

Before the establishment of the joint distribution, marginal distributions should be assumed first. GEV was utilized to construct the marginal distributions of wind speed and air temperature. Notably, for the sake of subsequent analysis, the air temperature in the cold months was taken inverse first.

Then, parameter estimations and goodness-of-fit tests were performed, and the results are shown in Table 4. The best-fitted model has the smallest RMSE (for CDF) and the largest R^2. It can be seen that all models have low RMSE values, which are less than 0.0453. In addition, all R^2 values are above 0.9763. These indicate that the selected models have satisfactory fitting results.

Table 4. Results of parameter estimations and goodness-of-fit tests.

Groups	Variables	Parameters			Goodness-of-Fit	
		k	σ	μ	RMSE (for CDF)	R^2
$G_{WS\text{-}H}$	Maximum wind speed	−0.0583	1.6205	8.2266	0.0266	0.9917
	Accompanying air temperature	−0.4111	4.6099	22.9894	0.0126	0.9981
$G_{WS\text{-}C}$	Maximum wind speed	0.0025	1.4850	6.7399	0.0293	0.9902
	Accompanying air temperature	−0.3688	6.0050	2.3208	0.0197	0.9956
$G_{AT\text{-}H}$	Accompanying wind speed	0.1568	1.2088	3.9948	0.0363	0.9853
	Maximum air temperature	−0.3017	3.0363	28.5297	0.0182	0.9960
$G_{AT\text{-}C}$	Accompanying wind speed	0.1639	0.9046	3.3832	0.0453	0.9763
	Minimum air temperature	−0.4000	5.6358	9.6102	0.0167	0.9968

To illustrate the fitting results more intuitively, the fitted curves and their corresponding frequency histograms are presented in Figure 6. Maximum wind speeds in Figure 6a,c

show the characteristics of Gumbel distribution, while accompanying wind speeds in Figure 6e,g follow a right-skewed Frechet distribution. Air temperatures in the hot months in Figure 6b,f follow a left-skewed Weibull distribution. On the contrary, air temperatures in the cold months in Figure 6d,h change from a right-skewed distribution to a left-skewed Weibull distribution by taking the opposite number.

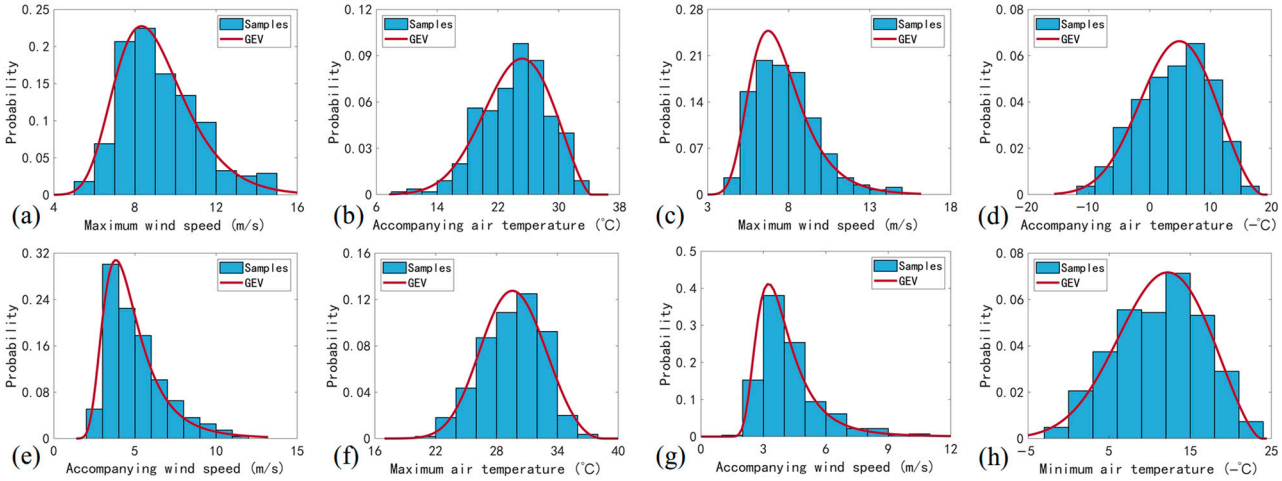


Figure 6. Fitting results for wind speed and air temperature: (**a**) maximum wind speed in $G_{WS\text{-}H}$; (**b**) accompanying air temperature in $G_{WS\text{-}H}$; (**c**) maximum wind speed in $G_{WS\text{-}C}$; (**d**) accompanying air temperature in $G_{WS\text{-}C}$; (**e**) accompanying wind speed in $G_{AT\text{-}H}$; (**f**) maximum air temperature in $G_{AT\text{-}H}$; (**g**) accompanying wind speed in $G_{AT\text{-}C}$; (**h**) maximum air temperature in $G_{AT\text{-}C}$.

3.4. Joint Distribution

Table 5 shows the results of parameter estimations and goodness-of-fit tests. Maximum likelihood estimation is introduced to implement parameter estimations. After that, RMSE and BIC are utilized to select the best fitted model. The best-fitted model should exhibit the lowest values of RMSE and BIC. The results indicate that the Frank Copula is the best fit in most of the cases. This is because the Frank Copula shows a more moderate tail dependence compared to other types of copulas. In most wind–temperature events, the tail dependence is not extremely strong or weak. The Frank Copula's ability to capture a middle-ground tail dependence can be beneficial. However, for maximum wind speed and accompanying air temperature in the cold months, the maximum wind speed and inversed accompanying low temperature show a pattern of upper-tail dependence. This kind of behavior is characteristic of the situations where the Gumbel Copula performs well.

Table 5. Results of parameter estimations and goodness-of-fit tests.

Groups	Copulas	Parameter	RMSE	BIC	Results
$G_{WS\text{-}H}$	Gumbel	1.0004	0.0153	−2300.3475	
	Clayton	0.0838	0.0112	−2473.6104	
	Frank	0.6462	0.0090	−2595.9585	adopted
$G_{WS\text{-}C}$	Gumbel	1.0130	0.0109	−2490.1116	adopted
	Clayton	1.45×10^{-6}	0.0109	−2489.6728	
	Frank	−0.0525	0.0109	−2487.1913	
$G_{AT\text{-}H}$	Gumbel	1.0000	0.0083	−2637.0771	
	Clayton	1.45×10^{-6}	0.0083	−2637.0793	
	Frank	−0.1716	0.0080	−2662.1704	adopted
$G_{AT\text{-}C}$	Gumbel	1.0000	0.0194	−2170.5376	
	Clayton	1.45×10^{-6}	0.0194	−2170.5400	
	Frank	−0.9474	0.0111	−2479.5611	adopted

To illustrate the fitting results more intuitively, P-P plots of the joint distributions were plotted, as shown in Figure 7. All scatters are closely distributed around the diagonal, suggesting that the expected models fit well with the empirical models. Figure 8 displays the JPDF of wind speed and air temperature in each group.

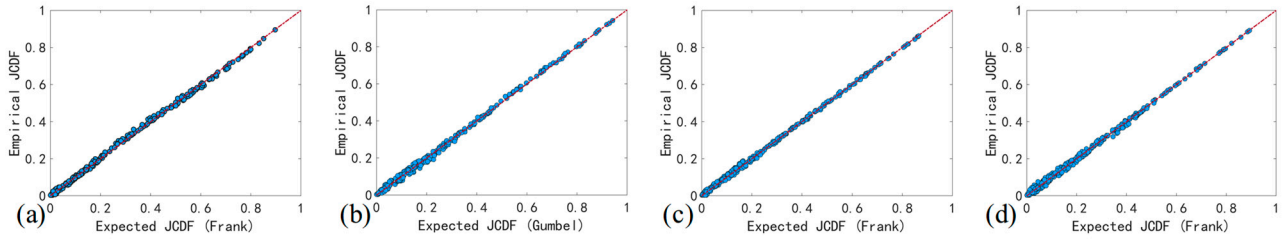


Figure 7. P-P plots of the selected joint distributions: (**a**) P-P plots of $G_{WS\text{-}H}$; (**b**) P-P plots of $G_{WS\text{-}C}$; (**c**) P-P plots of $G_{AT\text{-}H}$; (**d**) P-P plots of $G_{AT\text{-}C}$.

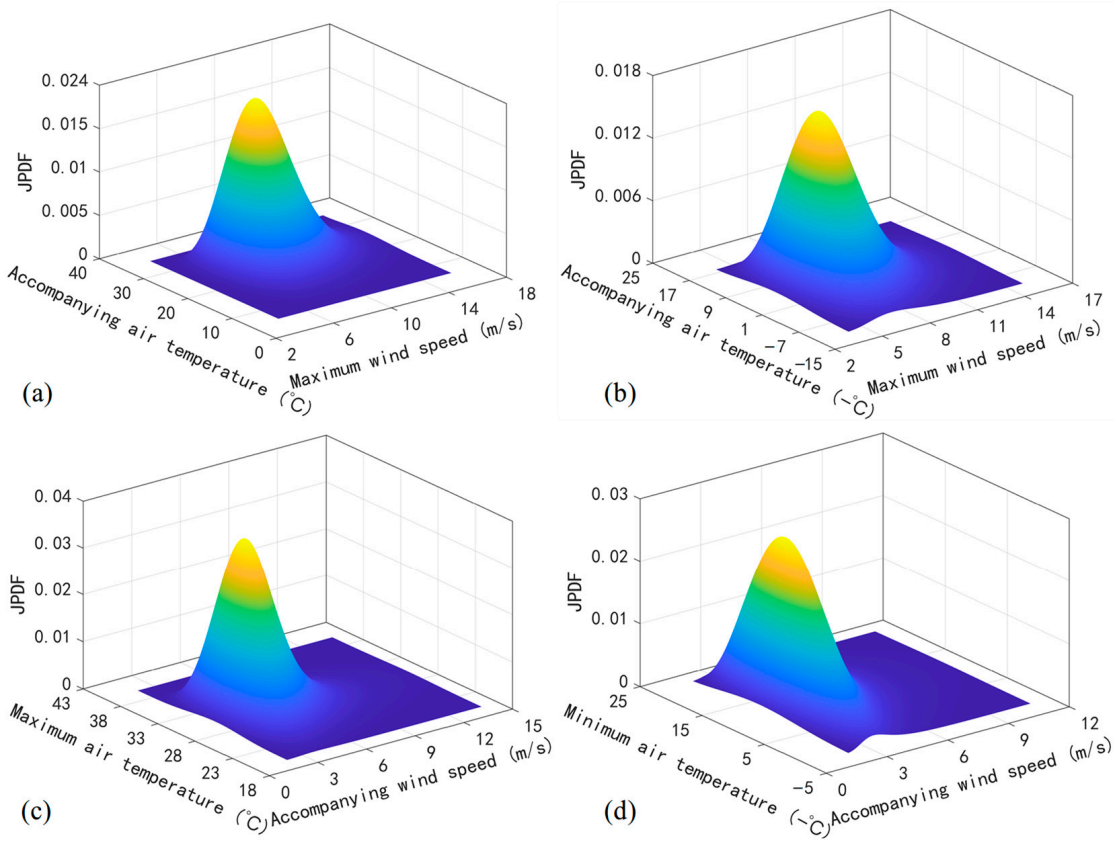


Figure 8. JPDF of wind speed and air temperature: (**a**) JPDF of $G_{WS\text{-}H}$; (**b**) JPDF of $G_{WS\text{-}C}$; (**c**) JPDF of $G_{AT\text{-}H}$; (**d**) JPDF of $G_{AT\text{-}C}$.

3.5. Joint Values and Combination Coefficients

The URVs of W1, W2, and maximum and minimum air temperatures were obtained first. Then, assuming a bivariate return period equals the univariate one, contour maps of the joint distributions were plotted, as shown in Figure 9. When one variable reaches its extreme, the other is reduced. And the joint values of wind speed and air temperature are acquired.

Next, the values were transformed into the joint values of wind and temperature actions. In this paper, wind speed is utilized to represent wind action, while uniform temperature action denotes temperature action. Uniform temperature action is defined as the difference between effective temperature and closure temperature. Effective temperature

takes maximum or minimum air temperature for CFST bridges [9]. Closure temperature adopts a unified 10 °C to facilitate the analysis.

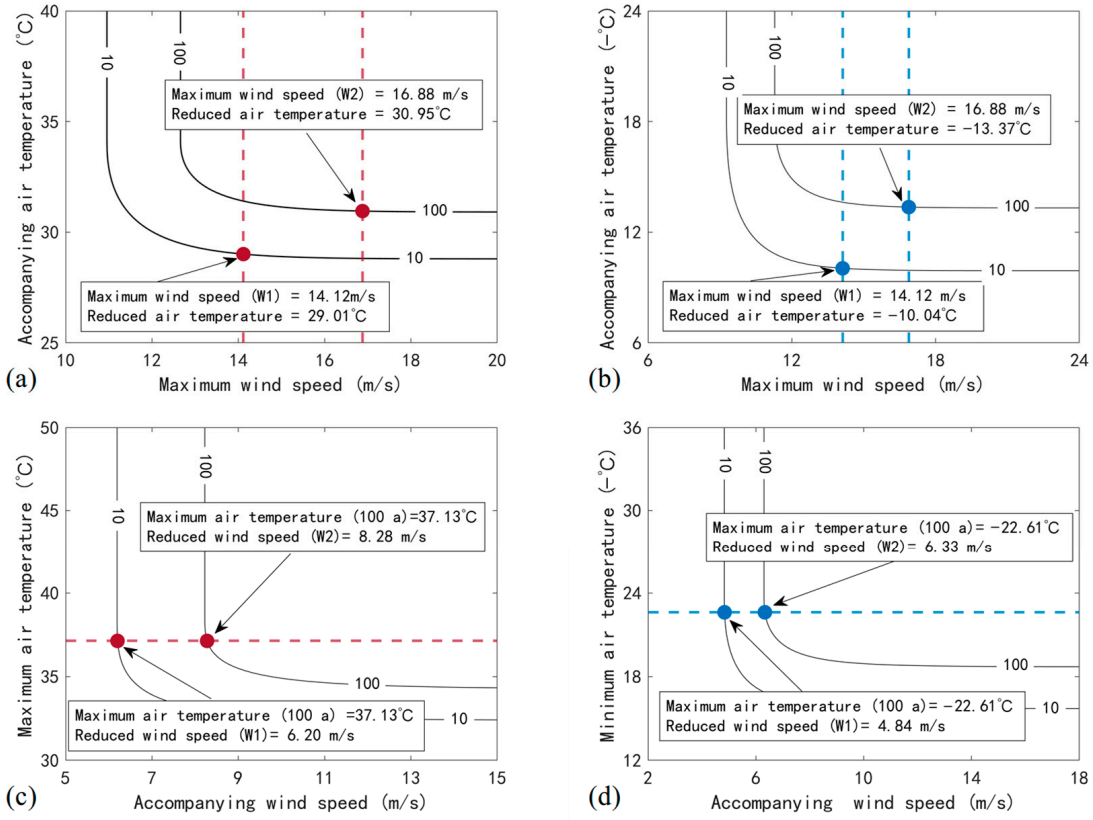


Figure 9. Contour maps of the joint distributions: (**a**) contours of $G_{WS\text{-}H}$; (**b**) contours of $G_{WS\text{-}C}$; (**c**) contours of $G_{AT\text{-}H}$; (**d**) contours of $G_{AT\text{-}C}$.

Table 6 shows the joint values and combination coefficients of wind and temperature actions. URVs of W1 and W2 adopt the values in $G_{WS\text{-}H}$, which are 14.12 and 16.88 m/s. This is because the representative values in $G_{WS\text{-}H}$ are larger than those in $G_{WS\text{-}C}$, and the former ones are more representative. The representative values of UHA and UCA with a return period of 100 a are 27.13 °C and −32.61 °C, respectively.

Table 6. Joint values and combination coefficients of wind and temperature actions.

Specified Actions	Specified Values	Reduced Actions	Reduced Values	Combination Coefficients
W1	14.12 m/s	UHA	19.01 °C (29.01 − 10)	0.70 (19.01/27.13)
		UCA	−20.04 °C (−10.04 − 10)	0.61 (−20.04/−32.61)
W2	16.88 m/s	UHA	20.95 °C (30.95 − 10)	0.77 (20.95/27.13)
		UCA	−23.37 °C (−13.37 − 10)	0.72 (−23.37/−32.61)
UHA	27.13 °C (37.13 − 10)	W1	6.20 m/s	0.44 (6.20/14.12)
		W2	8.28 m/s	0.49 (8.28/16.88)
UCA	−32.61 °C (−22.61 − 10)	W1	4.84 m/s	0.34 (4.84/14.12)
		W2	6.33 m/s	0.38 (6.33/16.88)

According to the combination coefficients in Table 6, it can be determined that the uniform temperature actions are less reduced when W2 is specified, compared with when W1 is specified. A similar situation occurs when the wind actions are reduced. In addition, the coefficients of UHA and UCA are 0.8 and 0.7 or so, indicating a 20~30% reduction

compared with their extremes, while those of wind action can be about 0.5, and the wind action is reduced greatly.

4. Discussion

A similar analysis was implemented for the remaining cities, and the combination coefficients of other typical cities in the YRB were obtained. The combination coefficients of other typical cities in the YRB are displayed in Table 7. For UHA, when W1 is specified, the combination coefficients range from 0.66 to 0.75; when W2 is specified, the coefficients are from 0.77 to 0.82. The maximum difference between the combination coefficients is no more than 0.1. The combination coefficients in cities with a temperate monsoon climate are relatively larger. On the other hand, for UCA, when W1 is specified, the combination coefficients range from 0.49 to 0.63; when W2 is specified, the coefficients are from 0.67 to 0.74. When W1 is specified, the variation is larger than when W2 is specified. The former can be up to 0.14. In addition, contrary to UHA, the combination coefficients of UCA in cities with a temperate continental climate are relatively larger. The reason lies in the fact that gales and extreme high temperature events are more likely to happen in areas with a monsoon climate in summer, while gales from inner Eurasia always bring frost to continental climate areas in winter.

Table 7. Combination coefficients in YRB.

Combinations	Specified Actions	Reduced Actions	Combination Coefficients (for Reduced Actions)							
			Xining	Lanzhou	Yinchuan	Hohhot	Taiyuan	Xi'an	Zhengzhou	Jinan
C1	W1	UHA	0.70	0.72	0.68	0.66	0.75	0.75	0.74	0.75
C2		UCA	0.61	0.53	0.58	0.63	0.59	0.55	0.54	0.49
C3	W2	UHA	0.77	0.80	0.78	0.77	0.82	0.82	0.82	0.82
C4		UCA	0.72	0.63	0.68	0.74	0.71	0.67	0.68	0.67
C5	UHA	W1	0.44	0.46	0.35	0.43	0.44	0.32	0.35	0.46
C6		W2	0.49	0.45	0.38	0.44	0.53	0.31	0.32	0.42
C7	UCA	W1	0.34	0.32	0.30	0.34	0.35	0.28	0.30	0.34
C8		W2	0.38	0.32	0.35	0.38	0.41	0.28	0.30	0.30

When it comes to W1 and W2, the difference between their combination coefficients is quite small, just 0.05 or so. When UHA is specified, the coefficients of wind actions are no more than 0.5, indicating a distinctive reduction for wind actions. Similarly, when UCA is specified, more reduction is found for wind actions, which can be up to 72%. From the above analysis, it can also be found that the reduction in wind actions is greater than that of uniform temperature actions.

To illustrate the effect of the combination coefficients, the finite element model of Jishixia Grand Bridge is developed, and it is shown in Figure 10. The 265 m span CFST truss arch bridge holds a rise–span ratio of 1/5.5. Eight CFST chords, numerous steel webs, and eighteen lateral and transverse bracings constitute the arch rib together. The CFST members are composed of 1000 mm outer diameter Q345 (yield strength 345 MPa) steel tubes with a thickness of 20 to 25 mm wrapped in C50 (compressive strength 50 MPa) micro-expansive concrete. The detailed material properties are displayed in Table 8. In the model, a CFST element is simulated with two parallel steel and concrete elements. A one-dimensional six-degrees-of-freedom beam element is used to simulate the steel and concrete elements. Fixed boundaries are assigned at the end of the arch rib.

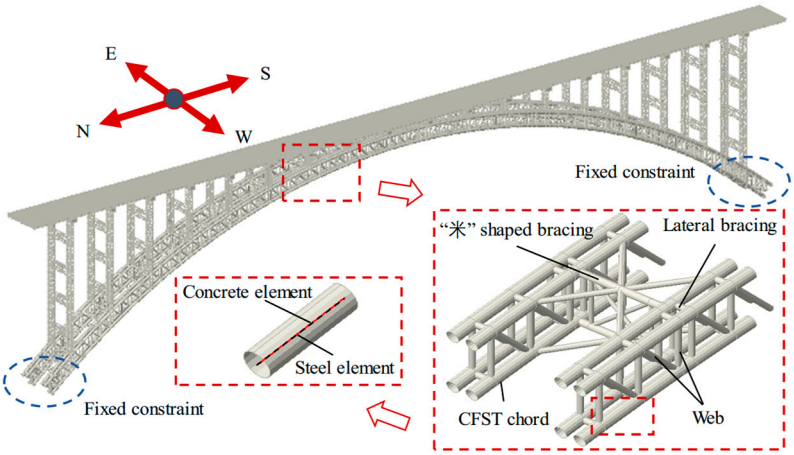


Figure 10. Finite element model of the CFST arch bridge.

Table 8. Material properties.

Material	Elastic Modulus (MPa)	Poisson's Ratio	Coefficient of Linear Thermal Expansion (1/°C)
Q345 steel	2.1×10^5	0.3	1.2×10^{-5}
C50 micro-expansive concrete	3.5×10^4	0.2	1.0×10^{-5}

The stress of the bottom chord at the springing segment in the northwestern arch was extracted and is shown in Table 9. To show the stress more intuitively, and in the interest of brevity, only the stress cloud maps of dead load and C1 in Xining are presented in Figure 11. A compressive stress of −77.80 MPa is caused by dead load. And the most unfavorable live load is −16.93 MPa. C1, C3, C5, and C6 produce tensile stress in the range from 16.93 to 39.69 MPa, while the others produce compressive stress ranging from −17.51 to −36.84 MPa. A difference in stress of about 20 MPa is found in the YRB for both compressive and tensile stress. The joint effects of wind and temperature are greater than those of live load but lower than the dead load effect. The maximum difference between live load and joint wind–temperature effect can reach 19.91 MPa for compressive stress. Meanwhile, the maximum compressive stress caused by the joint wind–temperature effect accounts for about 47% of the dead load effect. In addition, the stress in the combinations containing W2 is larger than that of W2. In addition, C3 and C4 are equipped with the maximum compressive and tensile stress in the eight combinations.

Table 9. Stress at arch springing (units: MPa).

Cities	Dead Load	Live Load	C1	C2	C3	C4	C5	C6	C7	C8
Xining	−77.8	−16.93	16.93	−17.51	20.20	−21.88	19.63	20.86	−22.72	−23.68
Lanzhou			20.39	−18.56	25.91	−24.79	21.95	23.69	−24.28	−25.57
Yinchuan			22.18	−23.07	30.00	−31.37	21.80	24.36	−26.04	−28.61
Hohhot			22.26	−27.17	30.98	−36.84	22.75	25.80	−30.51	−33.46
Taiyuan			21.91	−19.56	25.60	−24.39	22.76	24.64	−23.45	−24.83
Xi'an			24.34	−18.41	33.17	−27.84	23.18	25.38	−19.40	−21.48
Zhengzhou			27.21	−21.03	39.93	−34.49	25.10	28.28	−20.85	−24.16
Jinan			27.27	−20.85	39.69	−35.18	26.14	30.28	−22.65	−25.47

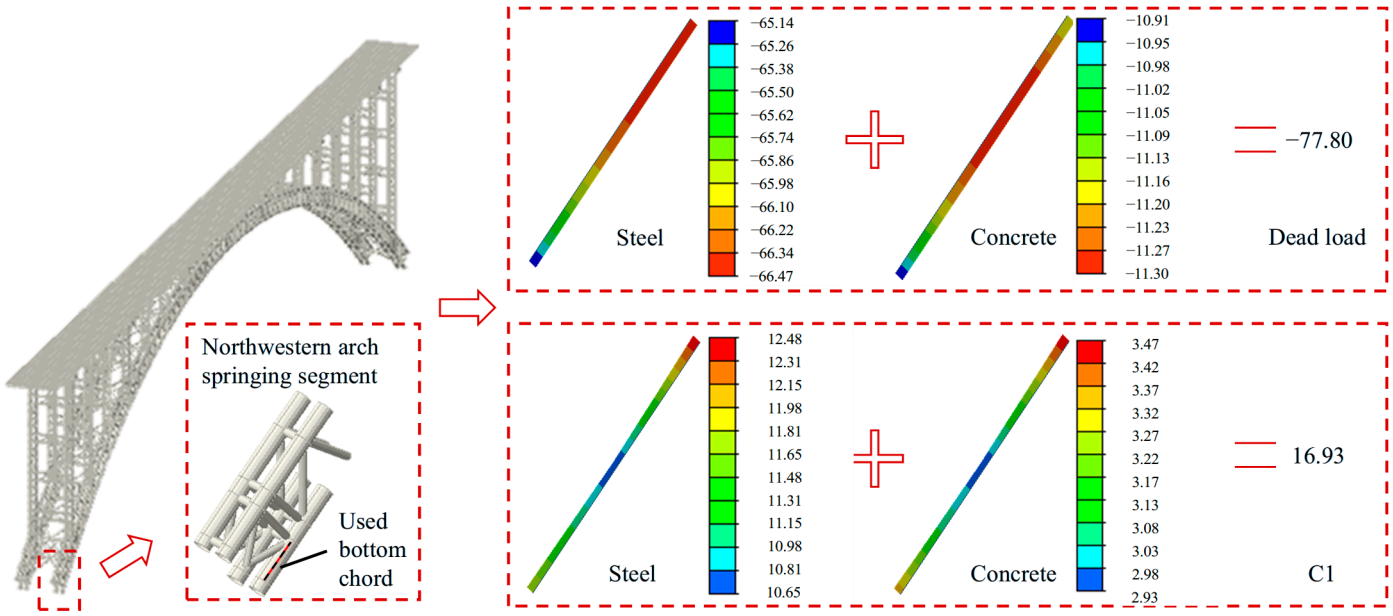


Figure 11. Stress in Xining (units: MPa).

In the analysis across the eight typical cities, it is observed that Zhengzhou holds the highest tensile stress, at 39.69 MPa, while Hohhot records the maximum compressive stress, at −36.84 MPa. These differences can be attributed to distinct local environmental factors that significantly influence the structural responses in these regions.

Zhengzhou is located in a region characterized by high temperatures and strong winds during the monsoon months, which contributes to elevated tensile stress. High temperatures exacerbate the expansion of materials. This thermal expansion, coupled with dynamic wind forces, leads to increased tensile stresses in structures. The design and material choices in Zhengzhou must therefore account for these extreme conditions to ensure structural integrity and safety.

Conversely, Hohhot's climatic conditions are markedly different. The city is frequently subjected to the effects of Mongolian cyclones during the winter, which bring severe cold weather and strong gales. These environmental factors play a critical role in the structural stress experienced in Hohhot. Cold temperatures lead to the contraction of materials, while the strong winds associated with cyclonic activity apply significant compressive forces on structures. The combination of these conditions results in the observed maximum compressive stress of −36.84 MPa. As such, the structural design in Hohhot must be adapted to mitigate the risks associated with such extreme compressive stresses, ensuring that bridges can withstand the harsh winter conditions prevalent in the region.

Figure 12 compares the stress in the proposed combinations and that in the specifications. The effects of the proposed combinations and those in the specifications are compared with the superimposition of the corresponding two effects. In most cases, the stress of the proposed combinations is less than that of the specifications. This is because the combination coefficients are below 0.75 of the value in the specification in most cases. However, in Xining and Lanzhou, for the specified temperature action cases, the response of the proposed combinations exceeds that of the specifications. And the maximum difference between the response of the proposed combinations and the specifications is 2 MPa or so in the same place, indicating that the General Specification underestimates the joint effects in some places. In the monsoon zone, including Xi'an, Zhengzhou, and Jinan, C6 and C8 exhibit much lower joint effects of wind and temperature compared to those in the

specifications. This yields too conservative strength margins, the maximum of which can be over 11 MPa.

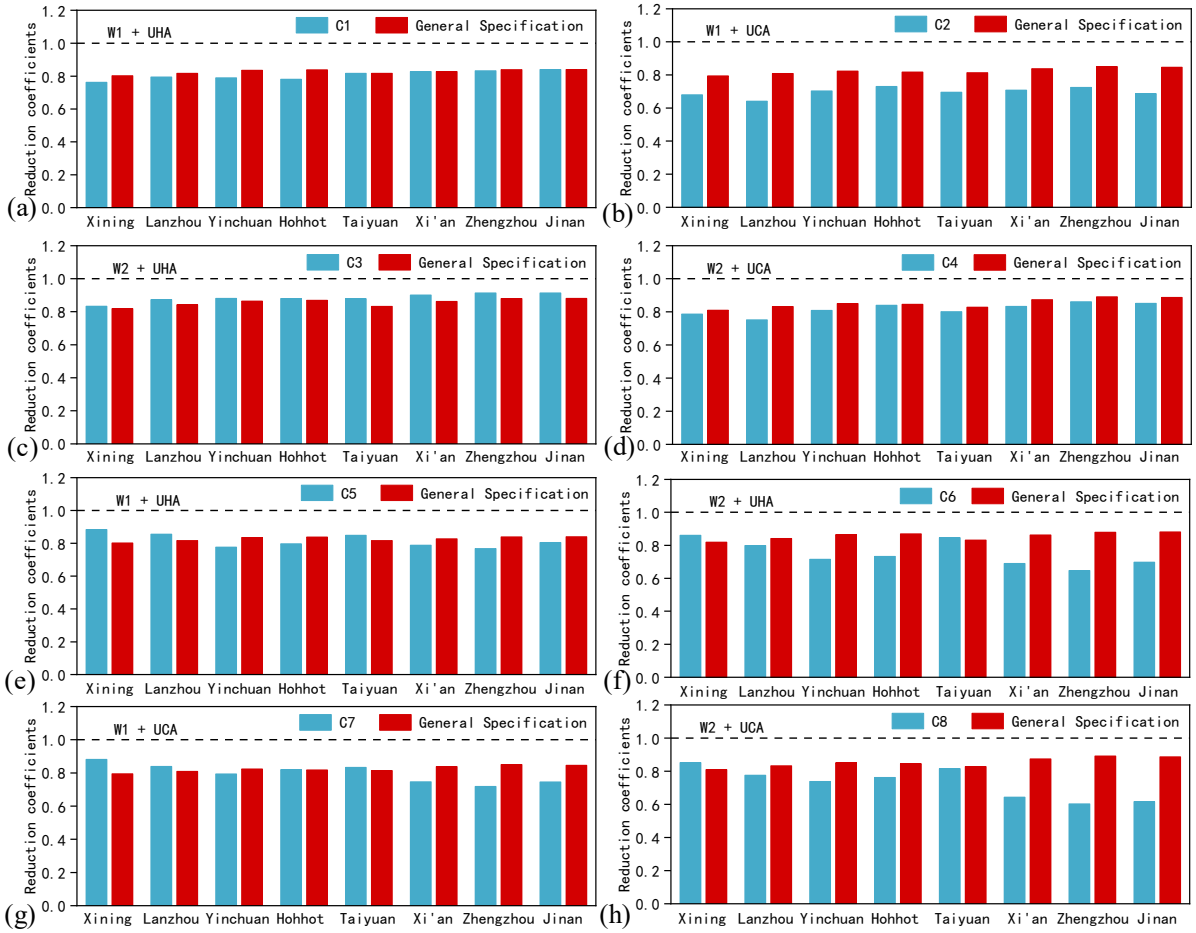


Figure 12. Stress comparisons between the proposed combinations and the specifications: (**a**) C1; (**b**) C2; (**c**) C3; (**d**) C4; (**e**) C5; (**f**) C6; (**g**) C7; (**h**) C8.

5. Conclusions

In this paper, the joint actions of wind and temperature are studied for long-span CFST bridges in the YRB. Eight typical cities are selected to investigate the typical wind and temperature performance of CFST bridges in the YRB. Some conclusive remarks are derived below:

(1) Eight typical cities are proposed to represent the typical wind and temperature characteristics of the YRB and are suitable for the analysis of the wind and temperature performance of CFST bridges.

(2) Archimedean Copulas provide an effective mathematical tool for the establishment of the joint distribution of wind speed and air temperature.

(3) Considering the correlation between wind and temperature actions, the joint wind–temperature actions can be obtained. They have different degrees of reduction compared with their URVs. When the wind actions adopt their URVs, the UHA and UCA will be reduced by 20 and 30%. Conversely, when uniform heating and cooling actions assume the URVs, the calculated wind speeds account for less than half of their URVs for both W1 and W2, and the reduction can even reach 70%.

(4) The wind and temperature response analysis shows that the presented joint actions and combination coefficients can expand the provisions in the General Specification

and are more suitable for wind and temperature response calculation and design for CFST arch bridges.

The temperature action in the joint wind–temperature action within this paper mainly concentrates on uniform temperature action. This provides a sound basis for subsequent study on the joint wind–temperature action incorporating the non-uniform part of temperature action.

Author Contributions: Conceptualization, J.L., H.W. and H.G.; methodology, J.L. and Y.M.; software, H.W.; validation, Z.M. and F.Z.; investigation, J.L.; writing—original draft, J.L.; writing—review and editing, H.W., Z.M., Y.L. and Y.M.; visualization, J.L. and H.W.; supervision, Y.L. All authors have read and agreed to the published version of the manuscript.

Funding: This study is funded by the Key R &D and transformation plan of Qinghai Province (Grant number: 2024-GX-117), which is gratefully acknowledged.

Data Availability Statement: Data are available upon reasonable request.

Conflicts of Interest: Author Guo Huajun was employed by the company Qinghai Provincial Transportation Construction Management Co., Ltd. The remaining authors declare that the research was conducted in the absence of any commercial or financial relationships that could be construed as a potential conflict of interest.

References

1. Li, J.W.; Xing, S.; Lv, S.C.; Li, Y. Flutter characteristics of bridges under non-uniform wind speed. *Structures* **2023**, *53*, 1–11. [CrossRef]
2. Zhou, M.; Fan, J.S.; Liu, Y.F.; Zhang, J.X.; Duan, X.J.; Lei, S.S. Non-uniform temperature field and effect on construction of large-span steel structures. *Automat. Constr.* **2020**, *119*, 103339. [CrossRef]
3. Liu, J.; Liu, Y.; Yan, X.; Zhang, G. Statistical investigation on the temperature actions of CFST truss based on long-term measurement. *J. Bridge Eng.* **2021**, *26*, 04021045. [CrossRef]
4. *JTG D60-2015*; General Specifications for Design of Highway Bridges and Culverts. China Communications Press: Beijing, China, 2015. (In Chinese)
5. *TB 10002-2017*; Code for Design on Railway Bridge and Culvert. China Railway Publishing House: Beijing, China, 2017. (In Chinese)
6. *JTG/T 3360-01-2018*; The Wind-resistant Design Specification for Highway Bridges. China Communications Press: Beijing, China, 2018. (In Chinese)
7. *EN 1991-1-5*; Eurocode 1: Actions on Structures—Part 1-5: General Actions—Thermal Actions. European Committee for Standardization (CEN): Brussels, Belgium, 2003.
8. Guo, Y.; Liu, H.B.; Wang, X.D.; Chen, Z.H. Study on basic temperature and wind-temperature load combination coefficient of steel structure. *Build. Struct.* **2017**, *47*, 6. (In Chinese) [CrossRef]
9. *GB 50923-2013*; Technical Code for Concrete-Filled Steel Tube Arch Bridges. China Planning Press: Beijing, China, 2013.
10. Salvadori, G.; Michele, C.D.; Kottegoda, N.T.; Rosso, R. *Extremes in Nature: An Approach Using Copulas*; Springer: Dordrecht, The Netherlands, 2007.
11. Genest, C.; Favre, A.C. Everything you always wanted to know about Copula modeling but were afraid to ask. *Hydrol. Eng.* **2007**, *12*, 347–368. [CrossRef]
12. Czado, C.; Thomas, N. Vine Copula based modeling. *Annu. Rev. Stat. Appl.* **2022**, *9*, 453–477. [CrossRef]
13. Bevacqua, E.; Maraun, D.; Hobæk Haff, I.; Widmann, M.; Vrac, M. Multivariate statistical modelling of compound events via pair-Copula constructions: Analysis of floods in Ravenna (Italy). *Hydrol. Earth Syst. Sci.* **2017**, *21*, 2701–2723. [CrossRef]
14. Sklar, M. Fonctions de Répartition à n Dimensions et Leurs Marges. Université Paris 8. 1959. Available online: https://hal.science/hal-04094463/document (accessed on 12 June 2023).
15. Zhang, F.; Cui, N.; Guo, S.; Yue, Q.; Jiang, S.; Zhu, B.; Yu, X. Irrigation strategy optimization in irrigation districts with seasonal agricultural drought in southwest China: A Copula-based stochastic multiobjective approach. *Agric. Water Manag.* **2023**, *282*, 108293. [CrossRef]
16. Varol, T.; Atesoglu, A.; Ozel, H.B.; Cetin, M. Copula-based multivariate standardized drought index (MSDI) and length, severity, and frequency of hydrological drought in the Upper Sakarya Basin, Turkey. *Nat. Hazards* **2023**, *116*, 3669–3683. [CrossRef]
17. Li, F.; Zheng, Q. Probabilistic modelling of flood events using the entropy Copula. *Adv. Water Resour.* **2016**, *97*, 233–240. [CrossRef]

18. Tang, X.S.; Li, D.Q.; Zhou, C.B.; Phoon, K.K. Copula-based approaches for evaluating slope reliability under incomplete probability information. *Struct. Saf.* **2015**, *52*, 90–99. [CrossRef]
19. Salvadori, G.; Tomasicchio, G.R.; D'Alessandro, F. Practical guidelines for multivariate analysis and design in coastal and off-shore engineering. *Coast. Eng.* **2014**, *88*, 1–14. [CrossRef]
20. Zhang, Y.; Beer, M.; Quek, S.T. Long-term performance assessment and design of offshore structures. *Comput. Struct.* **2015**, *154*, 101–115. [CrossRef]
21. Li, H.N.; Zheng, X.W.; Li, C. Copula-based joint distribution analysis of wind speed and direction. *J. Eng. Mech.* **2019**, *145*, 04019024. [CrossRef]
22. Huang, S.; Li, Q.; Shu, Z.; Chan, P.W. Copula-based joint distribution analysis of wind speed and wind direction: Wind energy development for Hong Kong. *Wind Energy* **2023**, *26*, 900–922. [CrossRef]
23. Chen, Q.; Yu, C.; Li, Y. General strategies for modeling joint probability density function of wind speed, wind direction and wind attack angle. *J. Wind Eng. Ind Aerod.* **2022**, *225*, 104985. [CrossRef]
24. Zhang, J.; Zhang, M.; Jiang, X.; Wu, L.; Qin, J.; Li, Y. Pair-Copula-based trivariate joint probability model of wind speed, wind direction and angle of attack. *J. Wind Eng. Ind Aerod.* **2022**, *225*, 105010. [CrossRef]
25. Zhang, H.; Liu, Y.; Deng, Y. Temperature gradient modeling of a steel box-girder suspension bridge using Copulas probabilistic method and field monitoring. *Adv. Struct. Eng.* **2021**, *24*, 947–961. [CrossRef]
26. Guo, F.; Zhang, S.; Long, Q.; He, C.; Yu, W.; Yi, L. Temperature Extreme Value Evaluation of Composite Beams Based on Copula Functions. *Case Stud. Constr. Mat.* **2024**, *21*, e03702. [CrossRef]
27. Wang, Z.W.; Zhang, W.M.; Tian, G.M.; Liu, Z. Joint values determination of wind and temperature actions on long-span bridges: Copula-based analysis using long-term meteorological data. *Eng. Struct.* **2020**, *219*, 110866. [CrossRef]
28. Zhang, W.M.; Wang, Z.W.; Liu, Z. Joint distribution of wind speed, wind direction, and air temperature actions on long-span bridges derived via trivariate metaelliptical and Plackett Copulas. *J. Bridge Eng.* **2020**, *25*, 04020069. [CrossRef]
29. Ding, Y.; Ye, X.-W.; Guo, Y. Copula-based JPDF of wind speed, wind direction, wind angle, and temperature with SHM data. *Probab. Eng. Mech.* **2023**, *73*, 103483. [CrossRef]
30. Zhou, R.; Jia, X.; Li, J.; Li, D.; Lu, P.; Zong, Z. Wind–Temperature Characteristics of a Cable-Stayed Bridge along the Yellow Sea under Superstrong Typhoon Lekima. *J. Bridge Eng.* **2024**, *29*, 04024086. [CrossRef]
31. Fu, G.; Chen, S.; Liu, C.; Shepard, D. Hydro-climatic trends of the Yellow River basin for the last 50 years. *Clim. Chang.* **2004**, *65*, 149–178. [CrossRef]
32. Orlando, M. Wind-induced interference effects on two adjacent cooling towers. *Eng. Struct.* **2001**, *23*, 979–992. [CrossRef]
33. China Meteorological Administration. *2024 Annual Bulletin of China 's Wind and Solar Energy Resources*; China Meteorological Administration: Beijing, China, 2025. (In Chinese)
34. Shi, D. *Practical Extreme Value Statistics Methods*; Tianjin Science and Technology Press: Tianjin, China, 2006. (In Chinese)
35. Joe, H. *Multivariate Models and Dependence Concepts*; Chapman and Hall: London, UK, 1997.
36. Nelsen, R.B. *An Introduction to Copulas*, 2nd ed.; Springer: New York, NY, USA, 2006. [CrossRef]
37. Deheuvels, P. La Fonction de Dépendence Empirique et Ses Propriétés, Un Test Non Paramétrique D'indépendence. *Acad. Roy. Belg. Bul. Cl. Sci.* **1979**, *65*, 274–292. Available online: https://www.persee.fr/doc/barb_0001-4141_1979_num_65_1_58521 (accessed on 12 June 2023).
38. Schwarz, G. Estimating the Dimension of a Model. *Ann. Stat.* **1978**, *6*, 461–464. Available online: https://www.jstor.org/stable/2958889 (accessed on 12 June 2023). [CrossRef]
39. Salvadori, G.; De Michele, C. Multivariate multiparameter extreme value models and return periods: A Copula approach. *Water Resour. Res.* **2010**, *46*, W10501. [CrossRef]

Disclaimer/Publisher's Note: The statements, opinions and data contained in all publications are solely those of the individual author(s) and contributor(s) and not of MDPI and/or the editor(s). MDPI and/or the editor(s) disclaim responsibility for any injury to people or property resulting from any ideas, methods, instructions or products referred to in the content.